The Soil Moisture and Ocean Salinity (SMOS) space mission: regularized inversion of dual-polarimetric interferometric data

ERIC ANTERRIEU
Observatoire Midi-Pyrénées
Laboratoire d'Astrophydique de Toulouse Tarbes
14, avenue Edouard Belin
31400 Toulouse - France

ALI KHAZAAL
Observatoire Midi-Pyrénées
Laboratoire d'Astrophydique de Toulouse Tarbes
14, avenue Edouard Belin
31400 Toulouse - France

Abstract: Synthetic Aperture Imaging Radiometers (SAIR) are powerful sensors for high-resolution observations of the Earth at low microwaves frequencies. Within this context, the European Space Agency is currently developing the SMOS mission devoted to the monitoring of Soil Moisture and Ocean Salinity at global scale from L-band space borne radiometric observations obtained with MIRAS, a two-dimensional Microwave Imaging Radiometer by Aperture Synthesis. This contribution is concerned with the reconstruction of radiometric brightness temperature maps from interferometric measurements obtained in the dual-polarimetric mode of MIRAS.

Key–Words: Remote sensing, Radiometry, Polarimetry, Synthetic aperture imaging, Inverse problems

1 Introduction

The two-dimensional L-band interferometer MIRAS (Microwave Imaging Radiometer by Aperture Synthesis) is the single payload of the SMOS (Soil Moisture and Ocean Salinity) space mission led by the European Space Agency [1] [2]. MIRAS consists of a Y-shaped interferometric array fitted with 69 equaly spaced antennas operating at 1.415 GHz (see Fig. 1).

Figure 1: Artiste view of SMOS.

The problem of retrieving the radiometric temperature distribution of a scene under observation from interferometric data has been widely addressed. It has been demonstrated that this problem is ill-posed and has to be regularized in order to provide a unique and stable solution [3]. This contribution extends the band-limited approach [4] to the case of the processing of dual-polarimetric data (namely those obtained in horizontal and vertical polarisations).

2 Theoretical framework

SAIRs devoted to Earth observation measure the correlation between the signals collected by pairs of spatially separated antennas which have overlapping fields of view, yielding samples of the visibility function V (also termed complex visibilities) of the brightness temperature distribution T of the observed scene.

2.1 Direct problem

The relationship between V and T has been recently revisited in order to take into account mutual effects of close antennas [5]. It is now given by:

$$V_{kl} = \frac{1}{\sqrt{\Omega_k \Omega_l}} \iint_{\|\boldsymbol{\xi}\|\leq 1} F_k(\boldsymbol{\xi}) \overline{F}_l(\boldsymbol{\xi}) \big(T(\boldsymbol{\xi}) - T_{rec}\big) \times \widetilde{r}_{kl}(t) \frac{\mathrm{e}^{-2\mathrm{j}\pi \mathbf{u}_{kl}\boldsymbol{\xi}}}{\sqrt{1-\|\boldsymbol{\xi}\|^2}} \mathrm{d}\boldsymbol{\xi}, \quad (1)$$

where $\mathbf{u}_{kl}$ is the spatial frequency associated with the two antennas $\mathcal{A}_k$ and $\mathcal{A}_l$ (namely, the spacing $\mathbf{d}_{kl}$ between $\mathcal{A}_k$ and $\mathcal{A}_l$ normalized to the central wavelength of observation λ_o), the components $\xi_1 = \sin\theta\cos\phi$ and $\xi_2 = \sin\theta\sin\phi$ of the angular position variable $\boldsymbol{\xi}$ are direction cosines in the SAIR reference frame (θ and ϕ are the traditional spherical co-

ordinates), T_{rec} is the physical temperature of the receivers, F_k and F_l are the normalized voltage patterns of the two antennas $\mathcal{A}_k$ and $\mathcal{A}_l$ with equivalent solid angles Ω_k and Ω_l (the overbar indicates the complex conjugate), $\widetilde{r}_{kl}$ is the fringe-wash function which accounts for spatial decorrelation effects, $t = \mathbf{u}_{kl}\boldsymbol{\xi}/f_o$ is the spatial delay and $f_o = c/\lambda_o$ is the central frequency of observation.

Denoting by ℓ the number of antennas, the number of complex visibilities V_{kl} (i.e. the number of baselines $\mathbf{d}_{kl}$) provided by the SAIR is equal to $n_b = \ell(\ell-1)/2$ when accounting for the hermitian property of (1). However, some spatial frequencies $\mathbf{u}_{kl}$ may be redundant since different pairs of antennas may lead to the same baseline. Since SAIR have limited physical dimensions, the spatial frequencies $\mathbf{u}_{kl}$ sampled by an interferometer are confined to a limited region of the Fourier domain: the experimental frequency coverage H. In the case of MIRAS, the visibility samples are obtained from raw data inside a star-shaped window over an hexagonally sampled grid $\mathbb{G}_{\mathrm{u}}$ in the Fourier domain [1]. Finally, for computational purposes, numerical integration is used to represent integral (1) as a summation over n^2 integrand samples, here the n^2 pixels of the spatial grid $\mathbb{G}_{\xi}$, the dual grid of $\mathbb{G}_{\mathrm{u}}$.

2.2 Inverse problem

The inverse problem aims at inverting the discrete version of (1) in order to retrieve T from V, i.e. solving the system

$$\mathbf{G}T = V, \tag{2}$$

where $\mathbf{G}$ is the discrete linear operator from the object space E into the data space F describing relation (1). Since the direct problem is stated *via* an integral equation, (2) does not usually have a straightforward solution. Moreover, since the dimension of E (the n^2 pixels used to sample T) is often larger than the dimension of F (the n_b samples of V), the linear system (2) is underconstrained with multiple solutions for T. As a consequence, the minimum of the least-square criterion

$$\min_{T\in E} \|V - \mathbf{G}T\|_F^2\,, \tag{3}$$

which is also the solution of the normal equation $\mathbf{G}^*\mathbf{G}T = \mathbf{G}^*V$, is therefore not unique because the square matrix $\mathbf{G}^*\mathbf{G}$ is singular. Thus, the inverse problem is ill-posed and has to be regularized in order to provide a unique and stable solution.

2.3 Band-limited regularisation

A new regularized approach has recently been proposed to the European Space Agency and selected for implementation in the ground segment prototype [4]. Referring to the limited resolution of the SAIR, this approach finds the temperature map T_r which has its Fourier transform confined to the experimental frequency coverage H. This band-limited solution realizes the minimum of the constrained problem

$$\begin{cases} \min\limits_{T\in E} \|V - \mathbf{G}T\|_F^2 \\ (\mathbf{I} - \mathbf{P}_H)T = 0 \end{cases} \tag{4}$$

where $\mathbf{P}_H$ is the projector onto the subspace $\mathcal{E}$ (of E) of the H-band limited functions. The unique solution of (4) is

$$T_r = \mathbf{U}^*\mathbf{Z}\mathbf{A}^+V, \tag{5}$$

where $\mathbf{A}^+$ is the More-Penrose pseudo-inverse of the rectangular matrix $\mathbf{A} = \mathbf{G}\mathbf{U}^*\mathbf{Z}$, $\mathbf{U}$ is the Fourier transform operator and $\mathbf{Z}$ is the zero-padding operator beyond H.

In order to filter out the Gibbs effects due to the sharp frequency cut-off associated to the experimental frequency coverage H, solution (5) is damped by an appropriate apodization function W [6]:

$$\mathcal{T}_r = \mathbf{U}^*\widehat{\mathbf{W}}\mathbf{U}T_r, \tag{6}$$

where $\widehat{\mathbf{W}}$ is the diagonal matrix whose non-zero elements are the values of $\widehat{W}$ in H. This map has to be compared to $\mathcal{T}_w = \mathbf{U}^*\widehat{\mathbf{W}}\mathbf{U}\,T$ (which is the "ideal" temperature map to be reconstructed and apodized with the same window W) and not to T (which is at a higher spatial resolution).

2.4 Extension to the dual-polarisation

In dual-polarimetric mode, MIRAS measures the brightness temperature in horizontal and vertical polarisations. Denoting by x and y the polarisations (in the SAIR reference frame) that are selected in each of the two receivers $\mathcal{R}_k$ and $\mathcal{R}_l$ involved in the particular baseline $\mathbf{d}_{kl}$, the dual-polarimetric version of (1) derived from [7] is given by the set of equations:

$$V_{kl}^x = \frac{1}{\sqrt{\Omega_k\Omega_l}} \iint\limits_{\|\boldsymbol{\xi}\|\le 1} \Big[C_k^x(\boldsymbol{\xi})\overline{C}_l^x(\boldsymbol{\xi})\big(T^x(\boldsymbol{\xi}) - T_{rec}\big) + X_k^x(\boldsymbol{\xi})\overline{X}_l^x(\boldsymbol{\xi})\big(T^y(\boldsymbol{\xi}) - T_{rec}\big)\Big]\, \widetilde{r}_{kl}(t)\frac{\mathrm{e}^{-2\mathrm{j}\pi\mathbf{u}_{kl}\boldsymbol{\xi}}\mathrm{d}\boldsymbol{\xi}}{\sqrt{1-\|\boldsymbol{\xi}\|^2}}, \tag{7}$$

$$V_{kl}^y = \frac{1}{\sqrt{\Omega_k\Omega_l}} \iint\limits_{\|\boldsymbol{\xi}\|\le 1} \Big[X_k^y(\boldsymbol{\xi})\overline{X}_l^y(\boldsymbol{\xi})\big(T^x(\boldsymbol{\xi}) - T_{rec}\big) + C_k^y(\boldsymbol{\xi})\overline{C}_l^y(\boldsymbol{\xi})\big(T^y(\boldsymbol{\xi}) - T_{rec}\big)\Big]\, \widetilde{r}_{kl}(t)\frac{\mathrm{e}^{-2\mathrm{j}\pi\mathbf{u}_{kl}\boldsymbol{\xi}}\mathrm{d}\boldsymbol{\xi}}{\sqrt{1-\|\boldsymbol{\xi}\|^2}},$$

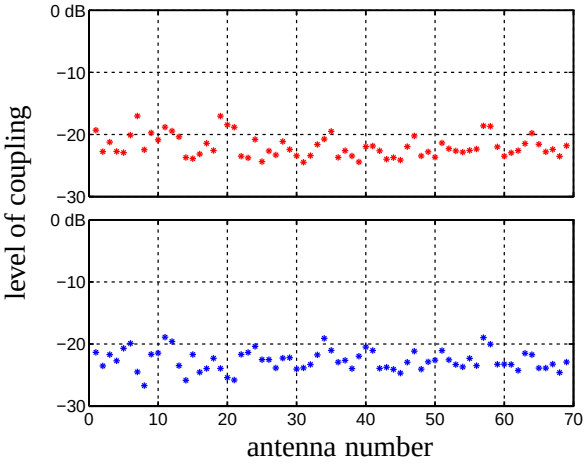

Figure 2: Level of coupling of the 69 antennas of MIRAS in x *(top)* and y *(bottom)* polarizations.

where T^x and T^y are the brightness temperature distributions of the observed scene in x and y polarisations. As demonstrated in [8], these brightness temperatures at antennas level are combinations of horizontal and vertical polarizations at Earth level. Since V^x and V^y samples depends on both T^x and T^y temperatures, the two previous equations are said to be coupled. Here, the level of coupling depends in both polarizations on the intensity level of the cross-polar voltage patterns X^x (resp. X^y) compared with the intensity level of the co-polar ones C^x (resp. C^y). As shown in Fig. 2 for the $\ell = 69$ antennas of MIRAS, this level of coupling varies from one antenna to another and from one polarization to another. On the average, it is about -21.9 dB for the x polarization and -22.7 dB for the y polarization.

Denoting again by $\mathbf{G}$ the 2×2 blocks modelling operator describing relations (7), the inverse problem (2) now reads:

$$\begin{pmatrix} \mathbf{G}_{xx} & \mathbf{G}_{xy} \\ \mathbf{G}_{yx} & \mathbf{G}_{yy} \end{pmatrix} \begin{pmatrix} T^x \\ T^y \end{pmatrix} = \begin{pmatrix} V^x \\ V^y \end{pmatrix}. \qquad (8)$$

According to (7), the diagonal blocks $\mathbf{G}_{xx}$ and $\mathbf{G}_{yy}$ only depend on the co-polar voltage patterns C^x and C^y whereas the off-diagonal ones, $\mathbf{G}_{xy}$ and $\mathbf{G}_{yx}$, only depend on the cross-polar voltage patterns X^x and X^y. Following the previous regularisation principle, the corresponding band-limited solutions read:

$$\begin{pmatrix} T_r^x \\ T_r^y \end{pmatrix} = \begin{pmatrix} \mathbf{U}^*\mathbf{Z} & 0 \\ 0 & \mathbf{U}^*\mathbf{Z} \end{pmatrix} \begin{pmatrix} \mathbf{A}_{xx} & \mathbf{A}_{xy} \\ \mathbf{A}_{yx} & \mathbf{A}_{yy} \end{pmatrix}^+ \begin{pmatrix} V^x \\ V^y \end{pmatrix}, \quad (9)$$

where $\mathbf{A}_{xx} = \mathbf{G}_{xx}\mathbf{U}^*\mathbf{Z}$, $\mathbf{A}_{xy} = \mathbf{G}_{xy}\mathbf{U}^*\mathbf{Z}$, $\mathbf{A}_{yx} = \mathbf{G}_{yx}\mathbf{U}^*\mathbf{Z}$ and $\mathbf{A}_{yy} = \mathbf{G}_{yy}\mathbf{U}^*\mathbf{Z}$ are the four blocks of the new 2×2 blocks matrix $\mathbf{A}$.

Depending on the level of coupling between equations (7), the off-diagonal blocks of $\mathbf{G}$ could be neglected. Consequently, the inverse problem (8) could be reduced to the regularization and the inversion of two independent problems of smaller size, namely $\mathbf{G}_{xx}T^x = V^x$ and $\mathbf{G}_{yy}T^y = V^y$. If this eventuality would happen, the off-diagonal blocks of $\mathbf{A}$ could also be neglected and the solutions (9) would reduce to:

$$\begin{aligned} T_r^x &= \mathbf{U}^*\mathbf{Z}\mathbf{A}_{xx}^+ V^x, \\ T_r^y &= \mathbf{U}^*\mathbf{Z}\mathbf{A}_{yy}^+ V^y. \end{aligned} \qquad (10)$$

Indeed, in such a situation, the computation of the More-Penrose pseudo-inverse $\mathbf{A}^+$ would reduce to the computation of $\mathbf{A}_{xx}^+$ and $\mathbf{A}_{yy}^+$, which is of course less time consuming. This eventuality is addressed in the next section with the aid of numerical simulations.

3 Numerical simulations

The results presented in this section are based on numerical simulations conducted within the frame of the SMOS project. The number of available complex visibilities V_{kl} is equal to $n_b = 2346$. However, some of the corresponding baselines $\mathbf{d}_{kl}$ are redundant and consequently there are only $n_f = 1395$ spatial frequencies in the star-shaped frequency coverage H.

Three reference radiometers are used for measuring the visibility function for the zero spacing [9]. The dimension of the sampling grids $\mathbb{G}_u$ and $\mathbb{G}_\xi$ has been fixed to $n^2 = 128 \times 128$. The size of the real-valued 2×2 blocks matrix $\mathbf{A}$ involved in the dual-polarization problem is therefore 9390×5582. As shown in Fig. 3, this matrix turns out to be block-diagonal dominant. As a consequence, provided that

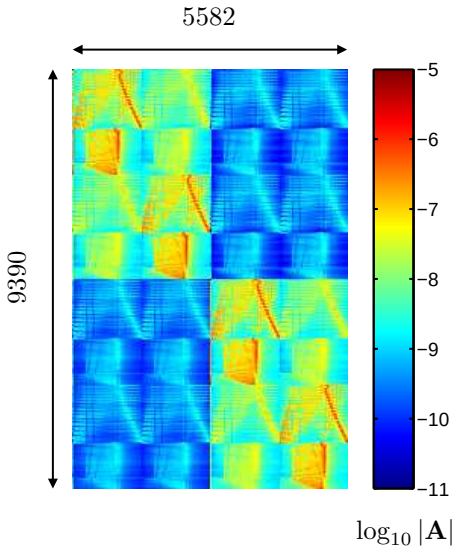

Figure 3: The regularized matrix $\mathbf{A}$ of MIRAS.

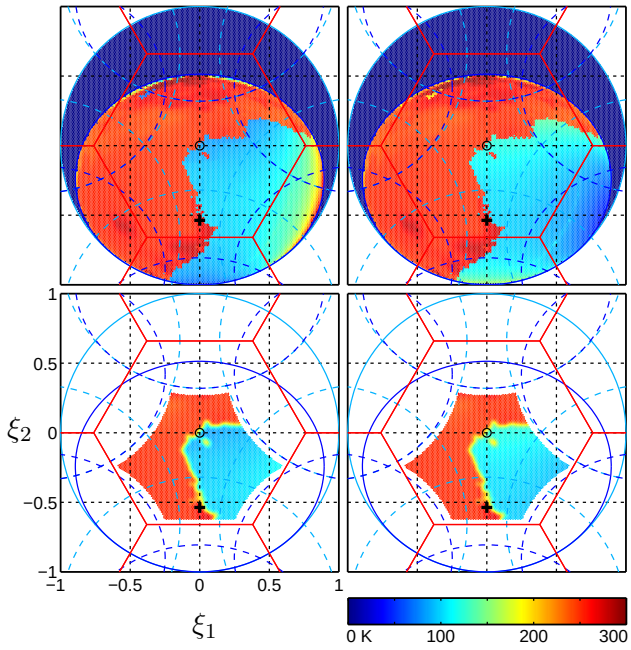

Figure 4: Example of a test scene in x *(left)* and y *(right)* polarizations at its highest level of resolution T *(top)* and the corresponding maps to be reconstructed $\mathcal{T}_w$ *(bottom)*.

the inversion process is still stable, the approximate solutions (9) should be very close to the complete ones (8).

Shown in Fig. 4 is an example of a test scene at its highest level of resolution as well as at the resolution level of the instrument and apodized with a Blackman window [6]. The synthesized field of view of MIRAS being subject to Earth and sky aliasing because of the spacing between the antennas [2], $\mathcal{T}_w^x$ and $\mathcal{T}_w^y$ are shown in that part of the synthesized field of view which is free from field aliasing whereas T^x and T^y are shown in the whole space in front of MIRAS.

Two sets of complex visibilities $V = \left(V^x, V^y\right)^t$ have been simulated from $T = \left(T^x, T^y\right)^t$:

- V_1 has been simulated without cross-polar gains so that V_1^x only depends on T^x and V_1^y only depends on T^y;
- V_2 has been simulated with both co-polar and cross-polar gains so that now V_2^x and V_2^y depend on T^x and T^y.

Then, three sets of maps $T_r = \left(T_r^x, T_r^y\right)^t$ have been retrieved:

- T_{1r} has been retrieved from V_1 with the corresponding independent reconstructions (10) since there is no coupling between V_1^x and V_1^y;
- T_{2r} has been retrieved from V_2 with the heavy reconstruction process (9) which involves the four blocks of $\mathbf{A}$ for taking into account the coupling between V_2^x and V_2^y;

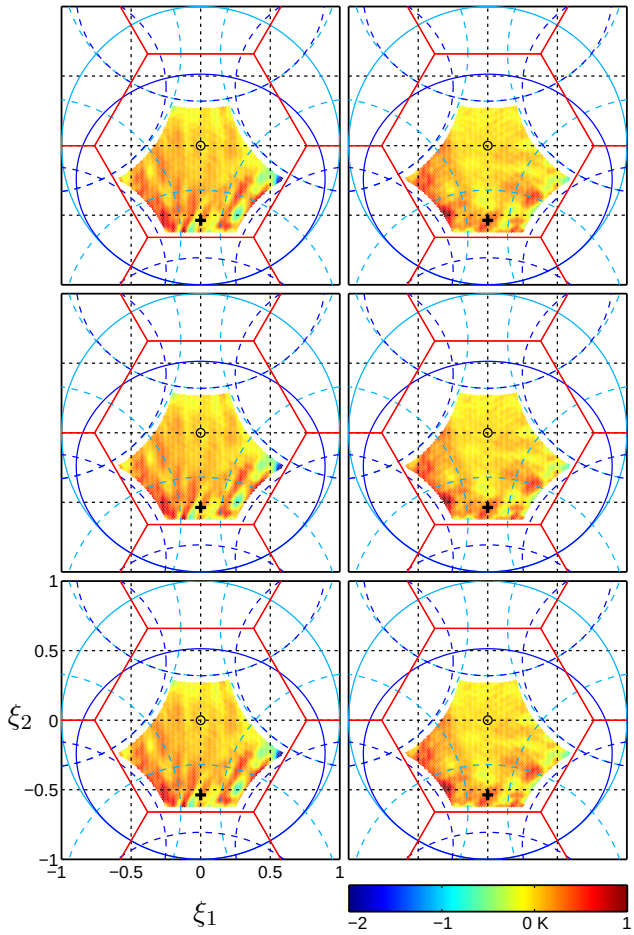

Figure 5: Example of error maps $\Delta\mathcal{T}_r$ in x *(left)* and y *(right)* polarizations for the retrieved maps T_{1r}, T_{2r} and T_{3r} *(from top to bottom)*.

- T_{3r} has also been retrieved from V_2 but with the light reconstructions (10) which do not take into account an eventual coupling between V_2^x and V_2^y.

The corresponding error maps $\Delta\mathcal{T}_r = \mathcal{T}_r - \mathcal{T}_w$ are shown in Fig. 5. Since $\Delta\mathcal{T}_{1r}$ and $\Delta\mathcal{T}_{2r}$ are almost identical, no size effect have affected the quality of the reconstruction (the bias $\overline{\Delta\mathcal{T}_r}$ and the standard deviation $\sigma_{\Delta\mathcal{T}_r}$ are of the same order: 0.23 K and 0.56 K, resp., for the x polarization, 0.14 K and 0.50 K, resp., for the y polarization). Moreover, since $\Delta\mathcal{T}_{2r}$ and $\Delta\mathcal{T}_{3r}$ are also almost identical, the coupling could be neglected. However, simulations with higher levels of coupling have shown that beyond -20 dB, the coupling should be taken into account in the reconstruction process.

4 Conclusions

This contribution was concerned with the reconstruction of brightness temperature maps from interferometric measurements provided by a SAIR. The band-

limited regularisation selected by the European Space Agency for the SMOS mission has been extended to the case of the processing of dual-polarimetric data. Depending on the level of coupling between the co-polar and cross-polar voltage patterns of the antennas, the retrieved maps are obtained either at the cost of the resolution of a large coupled system, if needed, or with the resolution of two independent problems of smaller size, if this coupling is negligeable. Provided that the coupling is taken into account when it is necessary, the quality of the retrieved dual maps does not change.

Acknowledgements: This work was supported by a grant from the Centre National d'Études Spatiales (CNES) and from the Région Midi-Pyrénées within the frame of the SMOS project.

References:

[1] M. Martin-Neira, Y. Menard, J.-M. Goutoule and U. Kraft, MIRAS, a two-dimensional aperture synthesis radiometer, *proc. IGARSS'94* (Pasadena, California, USA), vol. III, pp. 1323–1325, 1994.

[2] Y.H. Kerr, P. Waldteufel, J.-P. Wigneron, J.-M. Martinuzzi, J. Font and M. Berger, Soil Moisture Retrieval from Space: the Soil Moisture and Ocean Salinity (SMOS) mission, *IEEE Trans. on Geosc. and Remote Sens.*, 39(**8**), pp. 1729–1735, 2001.

[3] B. Picard and E. Anterrieu, Comparizon of regularized inversion methods in Synthetic Aperture Imaging Radiometry, *IEEE Trans. on Geosc. and Remote Sens.*, 43(**2**), pp. 218–224, 2005.

[4] E. Anterrieu, A resolving matrix approach for synthetic aperture imaging radiometers, *IEEE Trans. on Geosc. and Remote Sens.*, 42(**8**), pp. 1649–1656, 2004.

[5] I. Corbella, N. Duffo, M. Vall-llossera, A. Camps and F. Torres, The visibility function in interferometric aperture synthesis radiometry, *IEEE Trans. on Geosc. and Remote Sens.*, 42(**8**), pp. 1677–1682, 2004.

[6] E. Anterrieu, P. Waldteufel and A. Lannes, Apodization functions for 2D hexagonally sampled synthetic aperture imaging radiometers, *IEEE Trans. on Geosc. and Remote Sens.*, 40(**12**), pp. 2531–2542, 2002.

[7] M. Martin-Neira, S. Ribó and A.J. Martin-Polegre, Polarimetric mode of MIRAS, *IEEE Trans. on Geosc. and Remote Sens.*, 40(**8**), pp. 1755–1768, 2002.

[8] S. Ribó and M. Martin-Neira, Faraday rotation correction in the polarimetric Mode of MIRAS, *IEEE Trans. on Geosc. and Remote Sens.*, 42(**7**), pp. 1405–1410, 2004.

[9] A. Colliander, S. Tauriainen, T. Auer, J. Kainulainen, J. Uusitalo, M. Toikka and M. Hallikainen, MIRAS reference radiometer: a fully polarimetric noise injection radiometer, *IEEE Trans. on Geosc. and Remote Sens.*, 43(**5**), pp. 1135-1143, 2005.